J. Fluid Mech. (1966), *vol.* 24, *part* 1, *pp.* 65–88
Printed in Great Britain

A theoretical study of non-equilibrium blunt-body flows

By RAUL J. CONTI†
Department of Aeronautics and Astronautics, Stanford University

(Received 26 May 1965)

Non-equilibrium inviscid flows behind a spherical-segment shock wave are investigated with the method of series truncation. This semi-analytical technique developed at Stanford is based on a systematic co-ordinate-perturbation scheme. The flow variables are expanded in series in powers of the longitudinal curvilinear co-ordinate leading away from the stagnation point. The problem is thus reduced to one of numerical integration of ordinary differential equations for functions of the normal co-ordinate. Unlike the similar situation of the Blasius series in boundary-layer theory, the present scheme—having to deal with elliptic equations—must resort to series truncation. As a consequence, a truncation error is introduced. The present paper shows a simple way of reducing this error.

The simplified air chemistry adopted is based on non-equilibrium dissociation and recombination of oxygen diluted in inert nitrogen. A wide spectrum of non-equilibrium régimes is investigated for a fixed set of flight conditions. In particular, near-frozen flows are followed to the vicinity of the stagnation point through a region of large temperature and concentration gradients located near the body. This equilibrium-drive region, arising from the singular nature of the frozen limit, is studied in some detail.

1. Introduction

For some flight conditions frequently encountered in atmospheric entry, the heat involved in lagging chemical reactions is not small compared with the internal energy of the flow. Under these conditions chemical non-equilibrium effects can be expected to play an important role in determining flow properties such as temperature and species concentrations. It is now known that this is particularly true in the important class of flow problems associated with blunt-nosed vehicles. Strong shocks and embedded low-speed regions are distinctive characteristics of blunt-body flows, and several specialized techniques have been devised to deal with this problem. In the last few years several authors have incorporated vibrational or chemical relaxation into the following blunt-body theories: Newtonian approximation; inverse marching integration; boundary-layer-type techniques; stream-tube chemistry; shock-mapping technique; and method of integral relations. Each one of these methods has its own advantages and shortcomings. It would appear that a simple answer to this seemingly simple problem is yet to be found.

In the present investigation an effort is made to keep the treatment of the

† Now at the Lockheed Palo Alto Research Laboratory, Palo Alto, California.

problem as straightforward as possible, while using a minimum of restrictive assumptions. For this purpose the blunt-body flow including chemical non-equilibrium is analysed with the method of series truncation, with encouraging results. A flexible tool is developed that allows a comprehensive study of non-equilibrium régimes. Subsequent investigation of some of the salient flow features yields a better understanding of non-equilibrium flows in matters such as the chemical-relaxation behaviour in the vicinity of a stagnation point.

Some of the major features of non-equilibrium blunt-body flows were uncovered by Freeman (1958) when he used the Newtonian approximation—together with Lighthill's ideal dissociating gas and a rate equation of his own—to deal with chemically relaxing flow about a sphere. His numerical results indicated that significant changes in the flow could be induced by changing non-equilibrium régimes. The stand-off distance and shock shape were affected, as well as the chemical-species concentrations across the shock layer. Later research has confirmed these findings. In the same paper Freeman argued that the long local-residence time near the stagnation point would result in the flow achieving equilibrium in that region. This statement appears to be supported by his numerical results. In the present work more detailed evidence is exposed, which indicates that indeed this is the case. Freeman's Newtonian approximation, which does not allow for appreciable velocity changes along the body (or any other streamline), yields the result that chemical equilibrium persists along the body, a conclusion which is not borne out by later works, including the present paper. Ellington (1963) has recently extended the same method, and Blythe (1963) has used a similar approach to deal with vibrational relaxation.

In 1960 Lick used the inverse marching method (see Hayes & Probstein 1959) to deal with non-equilibrium blunt-body flows. This numerical method is exact in the sense that no simplications are introduced in the governing equations. An undesirable feature is that it suffers from numerical instability, resulting in the need for an integration mesh greater than a certain minimum. The corresponding lack of resolution is felt, for instance, in regions close to the body in near-frozen flows. This is perhaps the reason why Lick's results do not bridge the large apparent gap in surface values of density and temperature existing between frozen and near-equilibrium flows. Hall, Eschenroeder & Marrone (1962), Marrone (1963), and later on Lee & Chu (1964) have used the same technique to handle realistic, full-chemistry air models. These efforts have provided a good amount of information about reacting blunt-body flows.

In 1961 Chung and Murzinov independently used boundary-layer-type techniques to deal with relaxing flows on the stagnation streamline. Similar techniques were used before by Hayes, and Li & Geiger (see Hayes & Probstein 1959), in dealing with perfect-gas flows. Chung considered viscous, chemically reacting flow through a thin shock layer. Murzinov used the thin-layer assumption to deal with inviscid, vibrationally-relaxing flows.

The stream-tube-chemistry approach originated by Bloom & Steiger (1960) and Lin & Teare (1961) has been used in a large-scale sense to follow the chemical behaviour around bodies. Its delicacy for local application is doubtful, particularly in regions like the stagnation streamline.

In 1962 Gibson & Marrone introduced a flow-mapping technique to deal with non-equilibrium scaling in blunt-body flows. They established an approximate correspondence between the relaxing one-dimensional field behind a normal shock and the blunt-body flow field. This allowed them to compute blunt-body flows by reference to normal-shock solutions.

Dorodnitsyn's numerical method of integral relations (Hayes & Probstein 1959) has been used by several authors in the forms of scheme I (where the shock layer is divided into longitudinal strips) and scheme II (transversal strips) to study non-equilibrium flows. Shih & Baron (1964), and Springfield (1964) used a one-strip, scheme I formulation to deal with full-chemistry air models. Belotserkovskii & Dushin (1964) treated reacting oxygen flows by means of scheme II, on the grounds that it is better suited to follow the abrupt changes exhibited by non-equilibrium flow variables across the shock layer. In a later work Lun'kin & Popov (1964) obtained the same results by means of scheme I, used in a two-strip approximation with special handling of the chemical-rate equation.

A consistent picture emerges from the study of the above-mentioned authors. On one hand, the methods of Freeman, Chung, Murzinov, and Gibson & Marrone are characterized by carrying the analytic treatment to a certain extent, with the final results being obtained by more or less simplified numerical computations. These methods include restrictions of the type of the thin shock-layer assumption, local-similarity assumption, etc. Within these restrictions they are flexible techniques as is evidenced by the wide range of non-equilibrium conditions covered by these authors. On the other hand, the purely numerical approaches of Lick, Hall, Belotserkovskii, Shih & Baron, etc., while avoiding the use of simplifying assumptions, appear unable to cover such a wide range of non-equilibrium flows, as indicated by a lack of results in the near-frozen régimes.

The present semi-analytical approach is as free of restrictive assumptions as the numerical methods, and yet it retains the field resolution and ability to cope with large gradients of the more restricted techniques. This ability is exploited by investigating a wide spectrum of non-equilibrium régimes ranging from near-equilibrium to near-frozen flows. In particular, near-frozen flows are studied in the vicinity of the stagnation point, a region long neglected in previous works. Here the flow is found to be dominated by a drive toward equilibrium, a condition resulting in large temperature and species-concentration gradients. In this equilibrium-drive region the dynamics of the flow is practically uncoupled from the chemistry. This is a region of creeping motion and constant pressure, where chemical relaxation forces the flow toward equilibrium with a nearly linear relationship between temperature and degree of dissociation.

2. Analysis

The problem considered is the inverse one of plane or axisymmetric flow behind the front portion of a circular-cylindrical or spherical shock wave, respectively. The flow is assumed steady and adiabatic, and devoid of viscosity, heat conduction and diffusion. The free stream is assumed uniform, including its chemical composition. The co-ordinate system is shown in figure 1. The characteristic length is the radius of the shock $\tilde{r}_s$, to which all lengths are referred.

The physical flow variables are non-dimensionalized by reference to free-stream conditions. Thus, ρ and T are the density and temperature referred to ρ_∞ and T_∞; u and v are the velocity components along r and θ referred to U (the free-stream speed), and p is the pressure referred to $\rho_\infty U^2$. Time t is referred to the characteristic flow time $\tilde{r}_s/U$, and h is the static enthalpy referred to U^2.

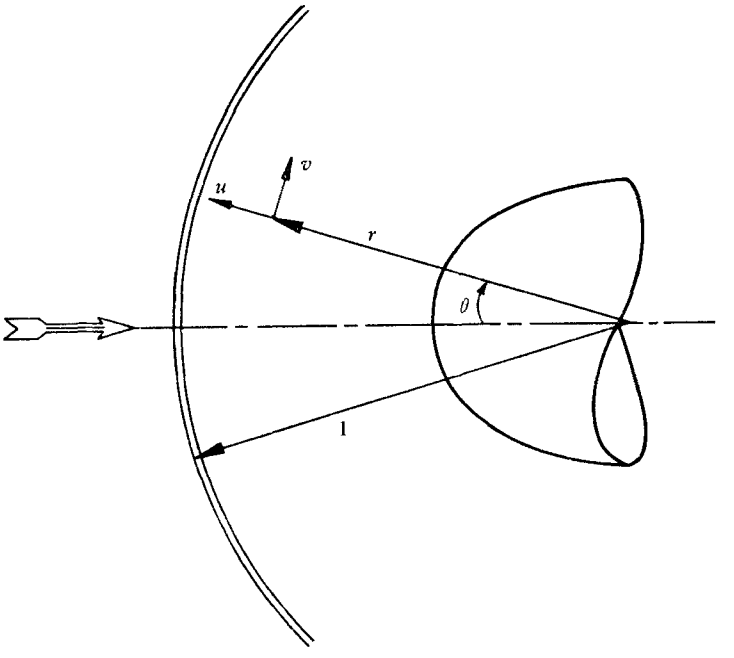

FIGURE 1. Polar co-ordinate system.

Subscripts b and s are used to denote conditions at the body and immediately downstream of the bow shock, respectively. Subscript e denotes equilibrium conditions.

Chemically relaxing gas model

Translational, rotational, and vibrational degrees of freedom are assumed in local equilibrium everywhere. Chemical non-equilibrium is allowed. The working gas is assumed to be a mixture of thermally perfect N_2, O_2, and O (or any other similar gases). Nitrogen is an inert diluent and oxygen undergoes dissociation–recombination reactions of the type

$$O_2 + P \rightleftarrows 2O + P,$$

where P represents, with the appropriate rate constant, N_2, O_2, or O. Under these conditions the chemical state of the system can be characterized by the degree of dissociation

$$\alpha = \frac{\text{mass of atomic oxygen}}{\text{total mass of oxygen}}.$$

The molecular-oxygen mass-fraction is then given by $1-\alpha$, and α lies in the range between zero and unity. This model is realistic for air under conditions such

that vibrational non-equilibrium and nitrogen dissociation are negligible. The equilibrium properties of the mixture are dependent upon an equilibrium 'constant' of the type

$$K(T) = AT^B \exp(-C/T),$$

and two true constants: a parameter β (the dilution ratio) equal to the mass ratio of nitrogen to oxygen, and δ, the ratio of molecular weights M_{O_2}/M_{N_2}. The constants A, B, and C are given in table 1. C is the dissociation energy per molecule referred to Boltzmann's constant and T_∞.

Altitude 30 km Flight speed 4·3 km/sec

$T_\infty = 230$ °K $\quad \rho_\infty = 1{\cdot}786 \times 10^{-2}$ kg/m^3 $\quad \alpha_\infty = 0$

$\beta = 3{\cdot}294$ $\quad \delta = 1{\cdot}142$ $\quad M_{O_2} = 32$ kg/kmol

Equilibrium constant $\quad K(T) = AT^B \exp(-C/T)$

Rate constant $\quad k(T) = DT^E \exp(-C/T)$

where

$$A = 1{\cdot}2 \times 10^6 (T_\infty)^B \text{ kmol/m}^3, \quad B = -\tfrac{1}{2}, \quad C = 5{\cdot}95 \times 10^4/T_\infty$$

Reaction partner P	D, m^3/(kmol.sec)	E	V
O_2	$1{\cdot}9 \times 10^{18}(T_\infty)^E$	$-1{\cdot}5$	$2{\cdot}25 \times 10^3/T_\infty$
N_2	$4{\cdot}75 \times 10^{17}(T_\infty)^E$	$-1{\cdot}5$	$3{\cdot}35 \times 10^3/T_\infty$
O	$6{\cdot}35 \times 10^{20}(T_\infty)^E$	$-2{\cdot}0$	—

TABLE 1. Numerical constants (MKS units used throughout).

For the present gas model the thermal and caloric equations of state are, respectively,

$$p/\rho = (1+\alpha+\beta\delta)\,RT, \tag{1}$$

$$\frac{h}{R} = [\tfrac{3}{2}\alpha + \tfrac{7}{2}(1+\beta\delta)]\,T + (1-\alpha)\frac{V_{O_2}}{\exp(V_{O_2}/T)-1} + \beta\delta\frac{V_{N_2}}{\exp(V_{N_2}/T)-1} + \alpha C, \tag{2}$$

where R is a dimensionless gas constant equal to the universal gas constant referred to $M_{O_2}(1+\beta)\,U^2/T_\infty$, and V is the characteristic temperature of molecular vibration referred to T_∞. In a non-equilibrium situation the rate of change of α is given by the chemical-rate equation which, in the present case, is

$$\frac{D\alpha}{Dt} = \left\{\frac{\tilde{r}_s}{U}\right\}\left\{\frac{\rho_\infty}{M_{O_2}(1+\beta)}[2\alpha k_O + (1-\alpha)\,k_{O_2} + \beta\delta k_{N_2}]\rho\right\}\left\{1-\alpha-4\frac{\rho_\infty}{M_{O_2}(1+\beta)}\frac{1}{K}\rho\alpha^2\right\}, \tag{3a}$$

where the quantity in the first curly brackets is a characteristic-flow time τ_f, the quantity in the second curly brackets is the reciprocal of a chemical local-relaxation time τ_{ch}, and the quantity in the last curly brackets is the function $\chi(\alpha, \rho, T)$, a measure of the departure from equilibrium. The expression for τ_{ch} contains three rate 'constants' of the Arrhenius type

$$k = DT^E \exp(-C/T),$$

where D and E are constants dependent upon the reaction, as shown in table 1. In the expression for χ the term $(1-\alpha)$ represents the forward (dissociation) reaction, and the term proportional to α^2 represents the three-body recombination

reaction. In a state of equilibrium the degree of dissociation is given by the law of mass action as

$$\frac{\alpha_e^2}{1-\alpha_e} = \frac{M_{O_2}(1+\beta)}{4\rho_\infty}\frac{K(T_e)}{\rho_e},$$

that is, in equilibrium $\chi = 0$, and this algebraic relation replaces the rate equation. In a general flow situation the non-equilibrium régime depends upon the ratio of characteristic-flow time to chemical-relaxation time. In the present work the level of chemical-relaxation time (dependent upon free-stream conditions) is kept constant. Different non-equilibrium régimes are obtained by changing the physical radius of the shock, $\tilde{r}_s$. Large values of $\tilde{r}_s$ (large flow times) correspond to régimes close to equilibrium, whereas small values of $\tilde{r}_s$ yield flows near the frozen limit ($\tilde{r}_s = 0$).

Flow equations and boundary conditions

Under the previous assumptions of steady, adiabatic, inviscid flow and in the polar co-ordinates of figure 1 the differential equations for plane ($\sigma = 1$) or axisymmetric ($\sigma = 2$) flow expressing conservation of mass, momentum, and energy are

$$\frac{\partial}{\partial r}[(\sin\theta)^{\sigma-1} r^\sigma \rho u] + \frac{\partial}{\partial\theta}[r^{\sigma-1}(\sin\theta)^{\sigma-1}\rho v] = 0, \tag{4}$$

$$\rho u\frac{\partial u}{\partial r} + \frac{\rho v}{r}\left(\frac{\partial u}{\partial\theta} - v\right) + \frac{\partial p}{\partial r} = 0, \tag{5}$$

$$\rho u\frac{\partial v}{\partial r} + \frac{\rho v}{r}\left(\frac{\partial v}{\partial\theta} + u\right) + \frac{1}{r}\frac{\partial p}{\partial\theta} = 0, \tag{6}$$

$$\rho u\frac{\partial h}{\partial r} + \frac{\rho v}{r}\frac{\partial h}{\partial\theta} - u\frac{\partial p}{\partial r} - \frac{v}{r}\frac{\partial p}{\partial\theta} = 0. \tag{7}$$

To these four equations are added the thermodynamic equations of state (equations (1) and (2)), and the chemical-rate equation in the form

$$u\frac{\partial\alpha}{\partial r} + \frac{v}{r}\frac{\partial\alpha}{\partial\theta} = \frac{\tau_f}{\tau_{ch}}\chi. \tag{3b}$$

The shock boundary conditions are obtained by applying the conservation equations across the specified shock wave, namely

$$\alpha_s = \alpha_\infty, \quad v_s = v_\infty, \quad u_s = u_\infty\epsilon, \quad \epsilon \equiv 1/\rho_s, \tag{8}$$

$$p_s = p_\infty + u_\infty^2(1-\epsilon), \tag{9}$$

$$h_s = h_\infty + \tfrac{1}{2}u_\infty^2(1-\epsilon^2). \tag{10}$$

This system is solved by iteration on ϵ and with the help of the equations of state, the iteration being necessary because of the gas imperfection introduced by molecular vibration. The body boundary condition is that of zero normal component of velocity at the surface of the body. The conservation, state and rate equations (equations (1) to (7)), together with the shock and boundary conditions, constitute a determinate system describing the flow in question exactly.

Method of solution

The problem is solved in semi-analytic fashion by the method of series truncation. This method was first applied to the blunt-body problem by Swigart (1962), and later improved by Kao (1964), Van Dyke (1964*a*, *b*) and the author (Conti 1964). It is based on a co-ordinate perturbation for small θ (or an equivalent co-ordinate) about the line of symmetry $\theta = 0$. A classical example of such a co-ordinate perturbation is found in boundary-layer theory in the form of the Blasius series (Schlichting 1960). There the stream function is formally expanded in series in powers of the longitudinal boundary-layer co-ordinate, with unknown functions of the normal co-ordinate alone as coefficients. Introduction of this series into the boundary-layer equation yields successive-order sub-problems in terms of ordinary differential equations for the unknown functions. These sub-problems are coupled, but each one can be solved exactly in terms of lower-order solutions. This establishes a one-way sequence in the solution of the original equation. Sub-problems are solved numerically by single-variable integration across the boundary layer. Thus, the longitudinal-co-ordinate dependence is by-passed in the actual process of solution while being retained in the original problem.

Essentially the same procedure is involved in the method of series truncation, with one major difference derived from the elliptic nature of the blunt-body equations. In physical terms, a co-ordinate perturbation such as described above fits naturally with problems exhibiting downstream influence only. Hence its success in dealing with the parabolic boundary-layer equation. The upstream influence associated with elliptic equations results in disruption of the orderly sequencing of sub-problems. However, approximate treatment of the elliptic equations as if they were parabolic is possible, and on this fact rests the method of series truncation. A more detailed description follows.

As a first step the problem is cast in a convenient form. The continuity equation (equation (4)) is used to define a stream function ψ such that

$$d\psi = (r\sin\theta)^{\sigma-1}(\rho v\,dr - \rho u r\,d\theta). \tag{11}$$

Then equations (5), (6), (7) and (3*b*) are manipulated algebraically with the help of equations (1), (2) and (11) to obtain a fifth-order system of four equations in the four unknowns ψ, p, T and α. The resulting momentum equations are of second order in ψ. This is the basic system of equations, and it is still exact.

Now the dependent variables are formally expanded in series in powers of $\sin\theta$ and $\cos\theta$. Thus,

$$\psi(r,\theta) = (\sin^{\sigma}\theta)\,[\psi_1(r) + \psi_2(r)\sin^2\theta + O(\sin^4\theta)], \tag{12a}$$

$$p(r,\theta) = p_1(r)\cos^2\theta + p_2(r)\sin^2\theta + O(\sin^4\theta), \tag{12b}$$

$$T(r,\theta) = T_1(r)\cos^2\theta + T_2(r)\sin^2\theta + O(\sin^4\theta), \tag{12c}$$

$$\alpha(r,\theta) = \alpha_\infty + \alpha_1(r)\cos^2\theta + \alpha_2(r)\sin^2\theta + O(\sin^4\theta). \tag{12d}$$

These are asymptotic expansions for small θ. Subscript 1 corresponds to the first-order problem, subscript 2 to the second-order problem, etc. The form of the expansions is suggested by various considerations. Expansion (12*a*) is dictated

by the symmetry and antisymmetry of the velocity components u and v, respectively, and the fact that v is small for small θ. The first term of (12*b*) is suggested by the generally observed behaviour of the pressure along the shock layer, with the second term being a perturbation thereof. Expansions (12*c*) and (12*d*) are tentative. Actually, the cosinusoidal-square variation of (12*d*) is too pronounced for a first approximation, in view of early chemical freezing.

Expansions (12) are substituted into the basic system of equations. Then, collection of terms in like powers of $\sin\theta$ yields a system of four equations of the following form:

$$\begin{aligned}
&[N_{11}(r, \psi_1, p_1, \alpha_1, T_1)] + [N_{12}(r, \psi_1, p_1, \alpha_1, T_1, \psi_2, p_2, \alpha_2, T_2)] \sin^2\theta + O(\sin^4\theta) = 0, \\
&\qquad\qquad \vdots \qquad\qquad\qquad\qquad\qquad\qquad\qquad\qquad\qquad\qquad \vdots \\
&[N_{41}(r, \psi_1, p_1, \alpha_1, T_1, p_2)] \\
&\qquad + [N_{42}(r, \psi_1, p_1, \alpha_1, T_1, \psi_2, p_2, \alpha_2, T_2, p_3)] \sin^2\theta + O(\sin^4\theta) = 0,
\end{aligned} \tag{13}$$

where the N_{ij} $(i = 1, 2, 3, 4; j = 1, 2, \ldots)$ are non-linear ordinary differential functions. The assumption that expansions (12) and equations (13) are valid for small but otherwise arbitrary θ yields $N_{ij} = 0$. In this notation i is a dummy index for the jth-order problem. Thus, the first-order problem is governed by the four differential equations $N_{i1} = 0$, the second-order problem by $N_{i2} = 0$, and so on. Notice that each of these problems contains a function belonging to the next-order one: in the first-order problem N_{41} contains $p_2(r)$, in the second-order problem N_{42} contains $p_3(r)$, etc. This establishes a two-way interdependence of the problems which is in striking correspondence with the physical upstream influence of the present subsonic flow. In contrast, the parabolic boundary-layer equation results in a self-contained first-order problem and higher-order problems solvable exactly in terms of the previous ones.

Clearly, then, the present case stands at the point where each sub-problem is an indeterminate one, having four equations for five unknowns. This situation is solved summarily in the method of truncations by setting the offending function equal to zero within each sub-problem. This is equivalent to successive truncations of series (12*b*); hence the name of the method. In this way the problem is rendered solvable but at the price of introducing an approximation. Obviously, more refined schemes are possible, such as assigning non-zero values to p_2, p_3, etc., on the basis of previous experience. Kao (1964) followed this line by arbitrarily extracting an equation for $p_2(r)$ from the second-order problem, with very good results. However, practical applications show that the simple device of truncation also gives very good results provided some care is exercised in formulating expansions (12).

In the actual solution by truncation the first truncation consists in solving $N_{i1} = 0$ with $p_2 = 0$ and appropriate boundary conditions. This yields an approximate solution to the first-order problem. The second truncation consists in solving the simultaneous system of eight equations $N_{i1} = N_{i2} = 0$ with $p_3 = 0$, which yields solutions to both the first- and second-order problems, now in the presence of a non-zero p_2. First-order solutions from both truncations are compared for convergence. The same process would be followed in the third trunca-

tion ($N_{i1} = N_{i2} = N_{i3} = 0$) and further ones until satisfactory numerical convergence is obtained.

Since algebraic complexity increases considerably with each successive truncation, it is important to realize the best possible convergence. To this end, the choice of variables and the form of expansions (12) are relevant. It is clear that, if p_2 is small, the error introduced by the first truncation will also be small and convergence will be improved. One way of ensuring that p_2 be small is to formulate expansion (12*b*) in such a way that the first term is a meaningful approximation to the actual situation at hand. In the present case this simple idea results in a significant improvement. This is illustrated by the limiting case of frozen (perfect-gas) flow. Here, only two variables need be expanded, and Swigart (1962) works with the stream function expanded as (12*a*) and density expanded in the form

$$\rho(r,\theta) = \rho_1(r) + \rho_2(r)\sin^2\theta + \ldots.$$

With the first term independent of θ, this is a good hypersonic approximation near the shock, but not on the body, where Newtonian pressure dictates a density proportional to $(\cos\theta)^{2/\gamma}$. In this context it is then difficult to represent density properly, and it must be discarded as a basic variable. Instead, the present expansion (12*b*) exploits the fact that pressure is well-represented by a cosinusoidal-square variation both near the shock and on the body. This results in a better first-truncation solution, as indicated by the stand-off distance, which in axisymmetric flow is in error by 30 % in the referenced work compared with 6 % in the present results. In the more extreme case of plane flow the corresponding figures are 500 and 17 %. It must be mentioned that in spite of this poor first truncation Swigart achieves good convergence in three or four truncations.

Further improvements are undoubtedly possible. Van Dyke (1964*a*) has suggested a modified form of expansions (12*a*, *b*) where, in the present case, sine functions are replaced by tangents. This introduces a change in the third truncation which cannot be appraised in the present two-truncation results. However, the equivalent modification for elongated bodies is crucial for a flow description far from the axis of symmetry.

Application to the present problem

For the present investigation two truncations were carried out following the general procedure described in the previous section. The first-truncation system ($N_{i1} = 0$) is (primes denote derivative with respect to r):

r-momentum

$$\left[\frac{r^{2\sigma}}{\sigma^2}\frac{p_1}{(1+\beta\delta+\alpha_\infty+\alpha_1)RT_1} - \frac{\psi_1^2}{p_1}\right]p_1' + \frac{\psi_1^2}{1+\beta\delta+\alpha_\infty+\alpha_1}\alpha_1' + \frac{\psi_1^2}{T_1}T_1' - \frac{\sigma}{r}\psi_1^2 + \psi_1\psi_1' = 0.$$

θ-momentum

$$\psi_1\psi_1'\left[-\frac{p_1'}{p_1} + \frac{\alpha_1'}{1+\beta\delta+\alpha_\infty+\alpha_1} + \frac{T_1'}{T_1}\right] + \psi_1\psi_1'' - \frac{(\psi_1')^2}{\sigma} + \frac{2-\sigma}{r}\psi_1\psi_1' + \frac{2r^{2(\sigma-1)}}{\sigma}\frac{p_1}{(1+\beta\delta+\alpha_\infty+\alpha_1)RT_1}(p_1 - p_2) = 0.$$

Energy

$$\frac{(1+\beta\delta+\alpha_\infty+\alpha_1)\,T_1}{p_1}\,p_1'-[\tfrac{3}{2}(\alpha_\infty+\alpha_1)+\tfrac{7}{2}(1+\beta\delta)+(1-\alpha_\infty-\alpha_1)\,F(V_{O_2})$$
$$+\beta\delta F(V_{N_2})]\,T_1'-\left[\tfrac{3}{2}T_1-\frac{V_{O_2}}{\exp(V_{O_2}/T_1)-1}+C\right]\alpha_1'=0,$$

where
$$F(V)=\left(\frac{V}{T_1}\right)^2\frac{\exp(V/T_1)}{[\exp(V/T_1)-1]^2}.$$

Rate

$$\sigma\psi_1\alpha_1'+r^\sigma\frac{\tilde{r}_s}{U}\frac{\rho_\infty}{M_{O_2}(1+\beta)}[2(\alpha_\infty+\alpha_1)\,k_O(T_1)+(1-\alpha_\infty-\alpha_1)\,k_{O_2}(T_1)$$
$$+\beta\delta k_{N_2}(T_1)]\left[\frac{p_1}{(1+\beta\delta+\alpha_\infty+\alpha_1)RT_1}\right]^2\chi_1=0,$$

where

$$\chi_1=1-(\alpha_\infty+\alpha_1)-\frac{4p_1}{(1+\beta\delta+\alpha_\infty+\alpha_1)\,RT_1}\frac{\rho_\infty}{M_{O_2}(1+\beta)}\frac{1}{K(T_1)}(\alpha_\infty+\alpha_1)^2,$$

and the rate constants k and equilibrium constant K are given in table 1. Notice the single appearance of p_2 in the last term of the θ-momentum equation.

This fifth-order system was reduced to a set of five first-order equations by introducing $\psi_1'(r)$ as a new variable and the identity $\psi_1'(r)=d\psi_1/dr$ as a new equation. Initial conditions (at the shock) were obtained as follows: $p_1(1)$, $T_1(1)$, and $\epsilon=1/\rho_s$ were calculated by introducing expansions (12*b*) and (12*c*) into the shock conservation equations (equations (9) and (10)) and iterating on ϵ across the shock. Conditions on the stream function follow from its definition (equation (11)), expansion (12*a*) and continuity of streamlines across the shock, which yield $\psi_1(1)=1/\sigma$ and $\psi_1'(1)=\rho_s$. The assumption of frozen chemical reactions across the shock ($\alpha_s=\alpha_\infty$), together with expansion (12*d*), yields $\alpha_1(1)=0$, which completes the set of initial conditions.

The second truncation was carried out by a straightforward continuation of the procedure as described earlier. In each truncation, the system of first-order ordinary differential equations was integrated numerically by means of a standard predictor–corrector routine for electronic digital computation. The IBM 7090 system of the Stanford Computation Center was used for this task. A first-truncation computation takes about 30 sec of machine time, and a second-truncation computation about 3 min.

Results are better presented when recast in terms of von Mises variables. This was found to be particularly helpful in describing the portion of the flow field lying near the body. As a first step the stream function is normalized by referring it to its value at the shock on the line $\theta=$ const. Thus, the normalized stream function is

$$\Upsilon=\frac{\psi(r,\theta)}{\psi(1,\theta)}=\frac{\sigma\psi(r,\theta)}{(\sin\theta)^\sigma}=\sigma[\psi_1(r)+\psi_2(r)\sin^2\theta+\ldots], \tag{14}$$

and it ranges from zero at the body to unity at the shock. The von Mises transformation is performed by letting Υ become an independent variable. In the

present case θ is retained as the second independent variable, and the dependent variables are expanded as

$$p(\Upsilon,\theta) = \bar{p}_1(\Upsilon)\cos^2\theta + \bar{p}_2(\Upsilon)\sin^2\theta + \ldots, \tag{15a}$$

$$T(\Upsilon,\theta) = \bar{T}_1(\Upsilon)\cos^2\theta + \bar{T}_2(\Upsilon)\sin^2\theta + \ldots, \tag{15b}$$

$$\alpha(\Upsilon,\theta) = \alpha_\infty + \bar{\alpha}_1(\Upsilon)\cos^2\theta + \bar{\alpha}_2(\Upsilon)\sin^2\theta + \ldots. \tag{15c}$$

The original space (r,θ) and the von Mises space (Υ,θ) are related by the common independent variable θ, and the following expansion for r,

$$r(\Upsilon,\theta) = \bar{r}_1(\Upsilon) + \bar{r}_2(\Upsilon)\sin^2\theta + \ldots. \tag{16}$$

Recasting of the results in von Mises variables is accomplished in two steps, by first introducing equation (16) into the right-hand side of equation (14) and re-expanding equation (14) in Taylor series about $\bar{r}_1(\Upsilon)$, which yields

$$\bar{r}_1(\Upsilon) = \psi_1^{-1}(\Upsilon/\sigma), \tag{17a}$$

and

$$\bar{r}_2(\Upsilon) = -\frac{\psi_2[\bar{r}_1(\Upsilon)]}{\psi_1'[\bar{r}_1(\Upsilon)]}. \tag{17b}$$

In the second step a similar substitution of equation (16) into equation (12*b*), and further expansion in Taylor series, gives

$$\bar{p}_1(\Upsilon) = p_1[\bar{r}_1(\Upsilon)], \tag{18a}$$

and

$$\bar{p}_2(\Upsilon) = p_2[\bar{r}_1(\Upsilon)] + r_2(\Upsilon).p_1'[\bar{r}_1(\Upsilon)]. \tag{18b}$$

Relations (18) also hold for temperature and degree of dissociation. Equations (16), (17), and (18) serve as recurrence formulae to transform the original results in the (r,θ)-space into the new results in the von Mises space (Υ,θ).

The body location and shape are found from data at the integration end-point, where $\Upsilon = 0$. Thus, from equation (16),

$$r_b(\theta) = r(0,\theta) = \bar{r}_1(0) + \bar{r}_2(0)\sin^2\theta + \ldots. \tag{19}$$

The quantity $\bar{r}_1(0)$ is equal to the r-co-ordinate of the stagnation point, where $\psi_1 = \Upsilon = 0$. The stand-off distance referred to the shock radius is $\Delta = 1 - \bar{r}_1(0)$. The quantity $\bar{r}_2(0)$ is obtained from equation (17*b*), used at the integration end-point.

3. Discussion of results

An example of axisymmetric flow was computed for the flight conditions and chemical data shown in table 1.† Two-truncation results are presented with the von Mises co-ordinate Υ as independent variable. Numerical integration and further transformations yield the functions $\bar{p}_1(\Upsilon)$, $\bar{p}_2(\Upsilon)$, etc., as described in the previous section. Then the full flow variables can be obtained throughout the flow field from equations (15).† These variables can be mapped into the (r,θ)-space by using equation (16). For this purpose the functions $\bar{r}_1(\Upsilon)$ and $\bar{r}_2(\Upsilon)$ are presented in figure 2. It can be seen that mapping involves a slight (order one) stretching of the r-co-ordinate, dependent from point to point upon Υ, θ, and the

† Plane flows were found to exhibit the same features as axisymmetric flows, with the former lying nearer the equilibrium limit.

non-equilibrium régime. The corresponding distortion is small, and all qualitative arguments to be presented apply equally well to both spaces.

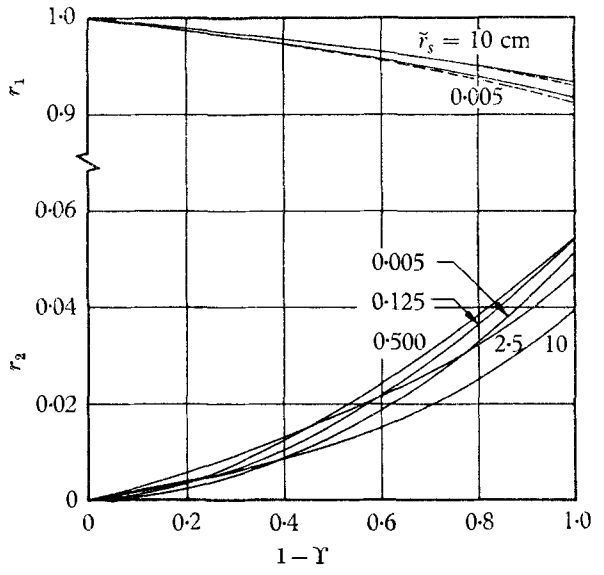

FIGURE 2. Mapping into physical space. Broken and solid lines are first and second truncations, respectively. The shock is at the origin of abscissae, the body at one.

Stagnation streamline

On the stagnation streamline, where $\theta = 0$, the full solution is given by the first-order variables as indicated by equations (15). The only approximation involved here is that derived from truncation. The truncation error is appraised from the numerical convergence of successive truncations. Although no mathematical study of this convergence has been made, the present reliance on two-truncation results is backed by solid evidence from previous research. In the limiting case of a perfect gas, Swigart (1962) and Van Dyke (1964*a*, *b*) have tested the method against a number of reliable results. On the stagnation streamline successive truncations converge monotonically to the correct values, with the difference between truncations becoming smaller with each step. Present results for frozen chemistry follow the same pattern. As an example, the stand-off distance in the first truncation is overestimated by about 6 %, and in the second truncation is obtained as accurately as is presently known. In the non-equilibrium régimes the convergence is expected to be qualitatively the same as in the frozen limit. Based on the previous considerations, results of the present investigation were regarded as satisfactory if the second truncation contributed only a small correction to the first one. This was always the case in the numerical computations. Results from the first and second truncations are plotted together for comparison.

Figure 3 shows the dimensionless pressure. As explained when discussing the rate equation, in the present work non-equilibrium régimes are characterized by the physical size of the shock radius, with large and small radii corresponding to near-equilibrium and near-frozen flows, respectively. The pressure is well behaved

across the shock layer, and second-truncation contributions are negligible. Non-equilibrium effects are small, but of the same order as the over-all pressure change.

Figure 4 shows the degree of dissociation, which has a possible range of zero to one (oxygen completely dissociated). Here non-equilibrium effects are drastic. In flows close to the equilibrium limit there is a rapid increase in dissociation behind the shock, followed by a near-equilibrium plateau extending to the body.

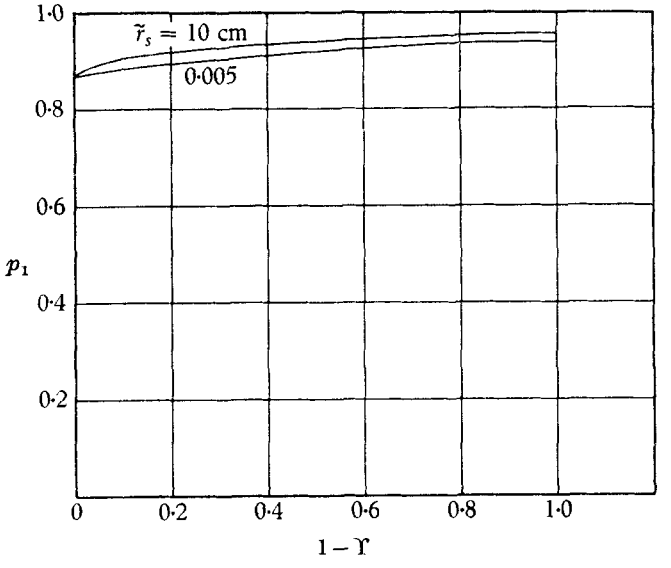

FIGURE 3. Dimensionless pressure on the stagnation streamline. Two truncations are indistinguishable to the present scale. The shock is at the origin of abscissae, the body at one.

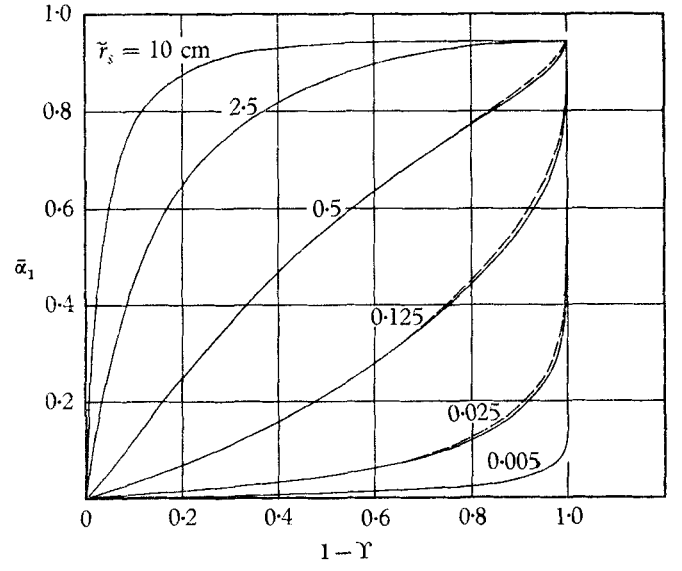

FIGURE 4. Degree of dissociation on the stagnation streamline. Broken and solid lines are first and second truncations, respectively. The shock is at the origin of abscissae, the body at one.

At the other extreme—near the frozen limit—dissociation remains close to the initial value through most of the shock layer, rising sharply toward equilibrium in the vicinity of the body. Concentration distributions in other non-equilibrium régimes are illustrated by the intermediate curves in the same figure.

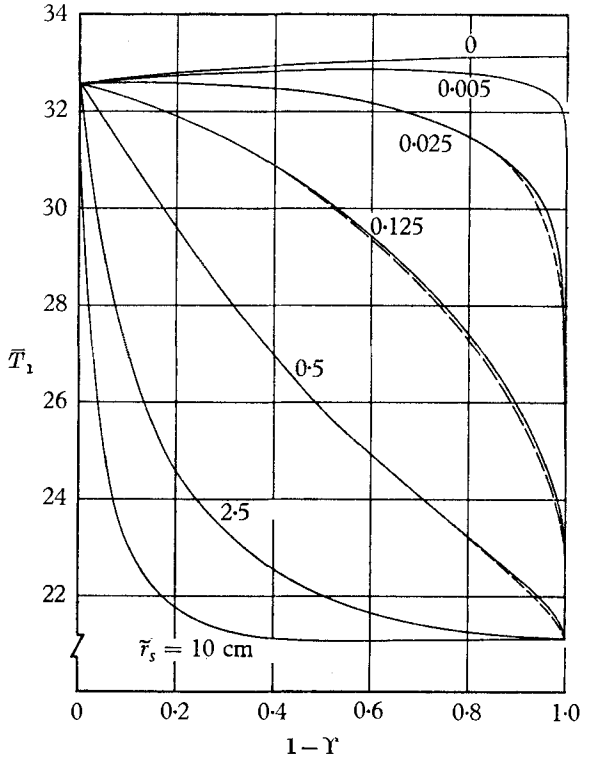

FIGURE 5. Dimensionless temperature on the stagnation streamline. Broken and solid lines are first and second truncations, respectively. The shock is at the origin of abscissae, the body at one.

The effects of this chemical behaviour upon other flow variables can be inferred from the fact that the kinetic energy of the flow is almost exhausted behind the shock. The energy involved in chemical reactions must then come almost entirely from the internal energy, which means that large differences in composition will be accompanied by large differences in temperature. This is illustrated in figure 5, where non-equilibrium solutions show that the temperature does follow the qualitative behaviour of the degree of dissociation. In particular, near-equilibrium flows exhibit low temperatures, whereas near-frozen flows maintain high temperatures through most of the shock layer, followed by the now familiar drive toward equilibrium near the body.

That equilibrium must be reached at the stagnation point is an intuitively appealing argument. It follows from the consideration that for round-nosed bodies it takes the flow an infinite time to reach the stagnation point from any finite distance. Hence, any non-zero chemical-relaxation time, however small, will eventually force the reaction to equilibrium. To the author's knowledge, this

has never been proved rigorously. However, the numerical results of Freeman (1958), Murzinov (1961), and Gibson & Marrone (1962) tend to indicate that this is the case. The same conclusion follows from the present work.

In the vicinity of the stagnation point a problem arises in that gradients of temperature and of concentration become very large. The present method to a certain extent overcomes this difficulty by affording arbitrarily small integration steps (in practice as small as one ten-millionth of the stand-off distance). However, in near-frozen flows straightforward integration to the body (adjusting the step size to maintain a constant machine-integration error) eventually ends in a situation where vanishing increments of the independent variable arrest one's progress, while temperature and composition still show finite changes. For these

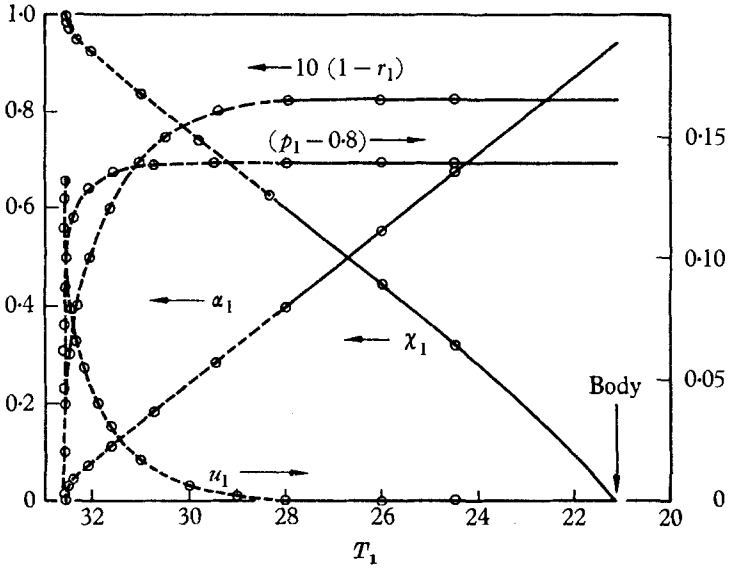

FIGURE 6. Stagnation equilibrium-drive region as a function of temperature for $\tilde{r}_s = 0{\cdot}025$ cm. Broken lines and circles indicate the original solution; solid lines indicate the transformed solution.

cases a different approach was clearly needed. This was provided by a simple transformation that changes the roles of the variables so that temperature becomes the independent variable and distance from the shock a dependent one. The impenetrability of the large-gradient region is overcome, since in the new transformed space all slopes remain of order one. Then integration in terms of temperature can proceed untroubled.

A typical case is shown in figure 6 with the new arrangement of variables. Several features are worth comment. The original solution is indicated by circles and broken lines, and is seen to overlap the new one smoothly and accurately. The pressure, velocity, and distance from the shock share a common trend: they approach constant values for a considerable range of temperatures. In fact, from this behaviour emerges a region, confined to the immediate neighbourhood of the stagnation point, of nearly constant pressure and slow motion, but sustaining considerable chemical change. In this region the degree of dissociation varies

almost linearly with temperature, as can be seen from the corresponding curve in figure 6. Results from all non-equilibrium régimes plot on this single curve. This is in accord with the fact that in the region in question velocity, velocity changes, and pressure changes, are higher-order quantities, and to first order the dynamics and chemistry of the flow are divorced. Because the characteristic effect in this region is the chemical relaxation toward equilibrium, it will here be referred to as the stagnation equilibrium-drive region.

Whether or not equilibrium is actually achieved at the stagnation point is a different question. In the transformed space (figure 6) the stagnation point $u = 0$ cannot be pinpointed for lack of numerical accuracy. However, in view of present results the following argument can be put forth: Equation (3) (the rate equation) shows that on the stagnation streamline, and for finite flow and chemical-relaxation times, the non-equilibrium function χ behaves like the product $u(\partial\alpha/\partial r)$. In near-frozen flows $|\partial\alpha/\partial r|$ increases monotonically as the stagnation point is approached. Provided this quantity remains non-zero, if equilibrium ($\chi = 0$) is attained anywhere, it can only occur at the stagnation point $u = 0$. Figure 6 (and all similar computations) show χ approaching zero unambiguously. Barring strange singularities at $u = 0$ or $\chi = 0$ or both, this is strong evidence that equilibrium is in fact attained at the stagnation point. For present purposes the stagnation point is assumed located at $\chi = 0$.

The near-frozen flows shown in figures 4 and 5 can be computed up to the stagnation point through the transformation described in the preceding paragraphs. The corresponding results show the stagnation equilibria to be grouped closely. They do not coincide, but differences appear only in the fourth significant figure for degree of dissociation, and the fifth figure for temperature. The pressure is more sensitive, as shown in figure 3.

Figure 5 illustrates the singular nature of the frozen limit. As the ratio of flow to chemical-relaxation time is continuously decreased, temperature profiles become fuller near the body but end conditions change insignificantly. When the frozen limit is reached (top curve) there is a sudden jump in the end condition. This behaviour is remindful of the singular limit of zero viscosity in boundary-layer theory or, for that matter, of the equilibrium limit at the shock in the present problem.

The stagnation equilibrium drive occurs in some region near the stagnation point, corresponding to the large gradients near $1 - \Upsilon = 1{\cdot}0$ in figures 4 and 5 The extent of this region varies with the non-equilibrium régime, but a qualitative idea of its thickness can be obtained by defining it as the distance from the body surface at which the slope dT_1/dr becomes greater than an arbitrarily chosen value. The thickness δ so defined appears consistently as shown on figure 7 for a typical value of dT_1/dr. Starting with zero thickness in the frozen limit ($\tilde{r}_s = 0$), the equilibrium-drive region quickly broadens to maximum thickness in some non-equilibrium régime, thereafter decreasing asymptotically to zero thickness in the equilibrium limit ($\tilde{r}_s \to \infty$). This implies that the equilibrium drive is present throughout the non-equilibrium régimes, resulting in large property gradients and over-all changes near the frozen limit, and still large gradients but vanishing over-all changes as the equilibrium limit is approached.

The stand-off distance is known to be sensitive to non-equilibrium changes. This is due to differences in density resulting from changing temperature and composition levels as flows range from equilibrium to frozen conditions. Present results for stand-off distance are shown in figure 8. It can be seen that near the equilibrium limit (where density levels are high) the stand-off distance is smallest, and weakly dependent upon the flow régime. Most of the change in stand-off distance occurs near the frozen limit. The present results include molecular vibration. Without vibration, the first and second truncations in the frozen limit yield stand-off distances of 0·1056 and 0·09988 of the shock radius, respectively.

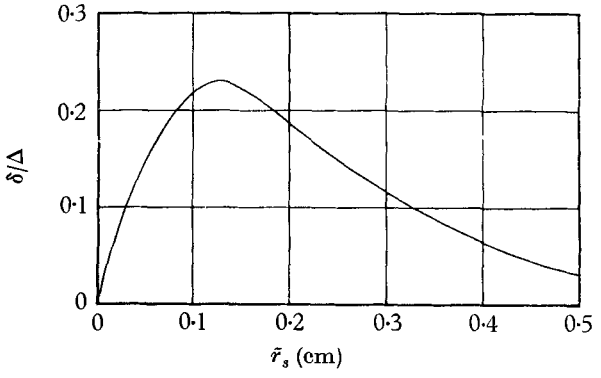

FIGURE 7. Thickness of equilibrium-drive region. The edge is defined as the point where $dT_1/dr = 140$.

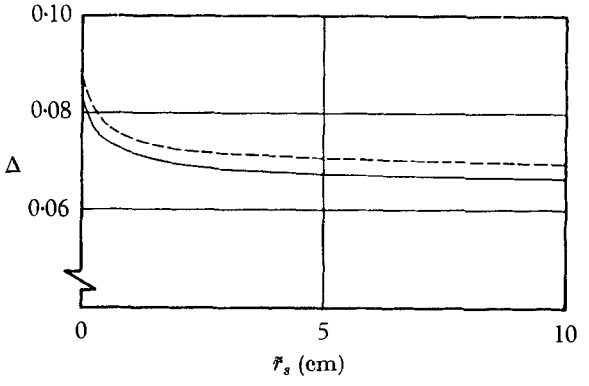

FIGURE 8. Stand-off distance referred to shock radius. Broken and solid lines are first and second truncations, respectively.

Flow field away from the axis of symmetry

Flow variables away from the axis are obtained from equations (15). In this representation the first-order terms include a cosinusoidal-square decay with θ, to which is added a second-order correction that grows like $\sin^2\theta$. In this section the second-order coefficients (subscript 2) are discussed. They represent departures from the postulated $\cos^2\theta$ variation of the first-order terms.

As indicated previously, expansions of the type of equations (15) are asymptotic for small θ. They provide a good representation of the flow field near the

stagnation streamline. As θ is increased they generally lose accuracy, and a larger number of terms is needed in the series. The extent of the region where a given number of terms provides a faithful representation of the flow field is not known *a priori*. However, an idea of the range of validity is obtained from Swigart (1962), who gets reasonable results near the sonic line with three truncations. Van Dyke's (1964*a*) more advanced formulation of the expansions leads to very good results in the sonic region in two truncations, for the test case of a paraboloidal shock in a perfect-gas flow. In the present investigation the effort was not directed toward the obtainment of particularly good results over the whole subsonic region, but rather toward a better understanding of non-equilibrium flows. Present results can be improved far from the axis by a systematic computation of more truncations, among other possibilities.

Figure 9 shows the pressure function $\bar{p}_2(\Upsilon)$ as obtained from the second truncation. Like the first-order coefficient $\bar{p}_1$, it is well behaved across the shock layer, and is fairly insensitive to non-equilibrium effects.

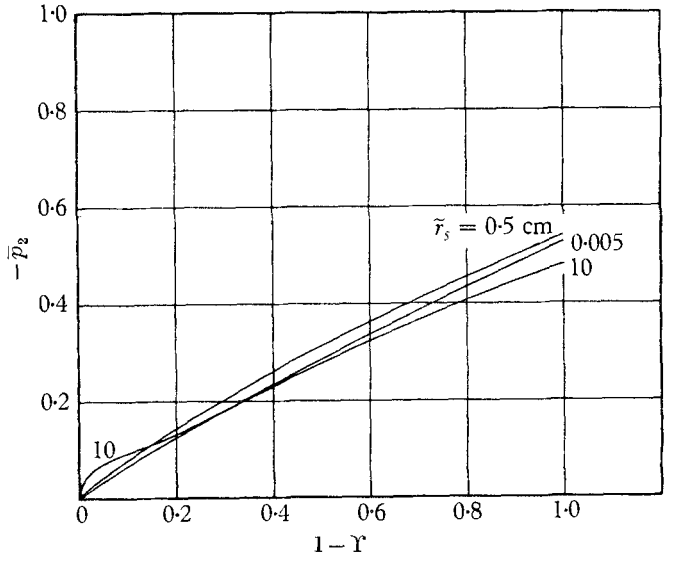

FIGURE 9. Dimensionless pressure function. The shock is at the origin of abscissae, the body at one.

Figure 10 shows the degree-of-dissociation function $\bar{\alpha}_2(\Upsilon)$. Here non-equilibrium effects are pronounced. In particular, as the frozen limit is approached large slopes are present near the body. This creates the same type of problem encountered on the stagnation streamline, and with worse computational difficulties. In perturbation schemes such as the present one singularities often tend to get worse as they spread to higher-order terms, which behave like derivatives of the previous ones. In the present case end-point values cannot be determined accurately in near-frozen flows. Within this limitation, values of $\bar{\alpha}_2$ of a score or more were sometimes obtained as the body was approached. This is within the restriction that $\bar{\alpha}_2$ should remain of order one. However, if these large values are not due to numerical inaccuracy, they imply (equation (15*c*)) that

within a short distance of the stagnation point the degree of dissociation becomes greater than unity, a situation which is physically impossible. It appears, then, that the radius of convergence of the present expansions is severely limited as the stagnation point is approached.

From the previous discussion it follows that in near-frozen flows there is a region of the flow field extending away from the stagnation point, and very near

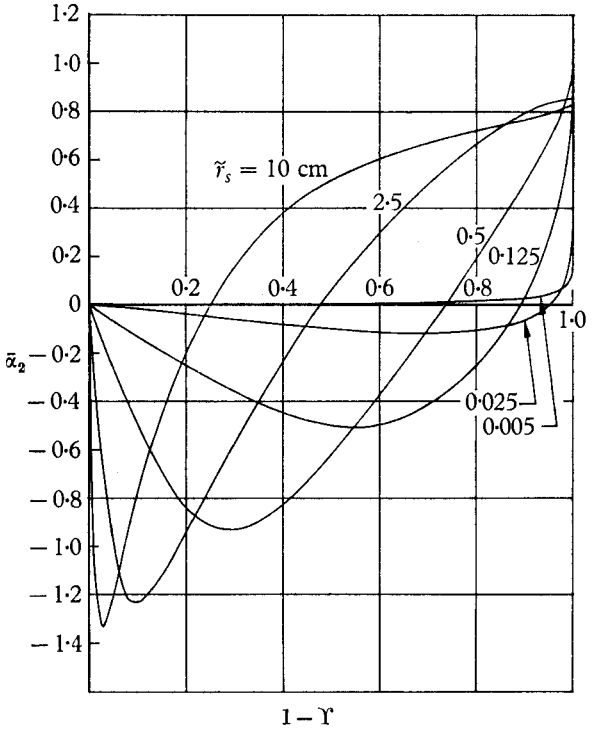

FIGURE 10. Degree-of-dissociation function. The shock is at the origin of abscissae, the body at one.

the body, which is not accessible with the present approach. As a consequence, the question is left unanswered as to whether an entropy layer exists near the body due to the stagnation equilibrium-drive phenomenon. The existence of such a layer can be argued on the ground that in near-frozen flows entropy-increasing chemical reactions are negligible everywhere, except for the body streamline and neighbouring ones that sustain the stagnation equilibrium drive. Under these conditions large entropy gradients could exist in the direction normal to the body surface. It would appear that the answer to this question should be sought by a different approach, such as the method of matched asymptotic expansions for the local treatment of perturbation singularities.

Figure 11 shows the temperature function $\bar{T}_2(\Upsilon)$. Similar comments apply to this variable. Figure 12 shows the flow variables on the body (referred to their stagnation-point values) in the non-equilibrium régimes corresponding to shock radii of 10 and 2·5 cm. Results are plotted up to forty degrees from the axis for

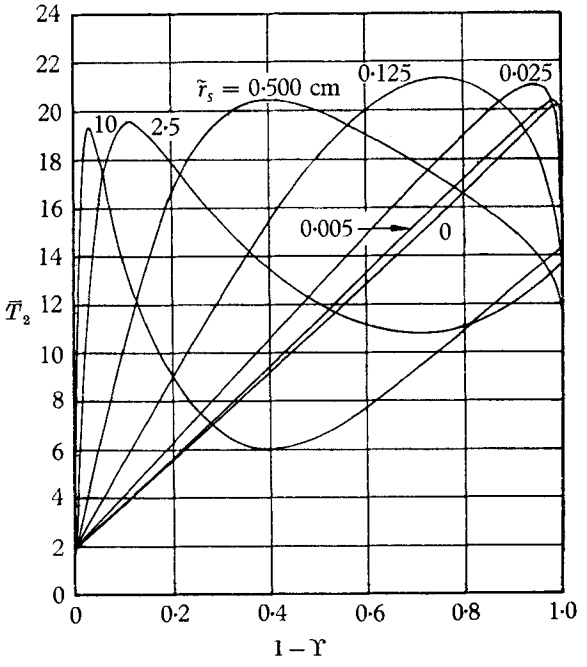

FIGURE 11. Dimensionless temperature function. The shock is at the origin of abscissae, the body at one.

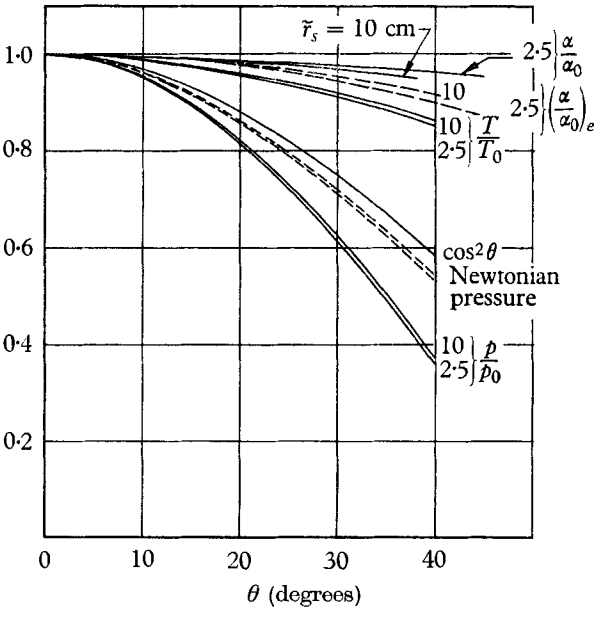

FIGURE 12. Flow variables on the body surface referred to their stagnation-point values.

the purpose of showing trends only. This does not reflect an expected range of validity. In broken lines are shown the Newtonian pressure, and the degree of dissociation for local equilibrium. The latter was computed by means of the law of mass action, from local values of pressure and temperature. Notice that the non-equilibrium composition lags local equilibrium values by amounts that increase in the direction of the frozen limit. The composition curves are generally flat, an indication of early chemical freezing.

Axisymmetric body shapes are given by equation (19) and can be represented graphically on any plane of symmetry as shown in the insert of figure 13. Both the location and the shape of the body are sensitive to the non-equilibrium régime. The location is given by the stand-off distance $\Delta = 1 - \bar{r}_1(0)$ which was discussed previously (see figure 8). The shape is represented by $\bar{r}_2(0)$, which is shown in figure 13. As non-equilibrium flows depart the frozen limit the body recedes more from a circle concentric with the shock. There is a maximum, followed by the reverse trend: as the equilibrium limit is approached the body moves back toward a circle concentric with the shock.

Comparison of results

It has been mentioned elsewhere that in the frozen (perfect-gas) limit the present method has been tested in a number of cases and found to give very good results over a large portion of the subsonic flow region. In non-equilibrium régimes comparison of results is more difficult. Notoriously lacking in exact scaling, non-equilibrium flows depend upon a number of parameters that must be duplicated for the purpose of comparison. To make matters worse, chemical gas models vary with the author, and chemical–kinetic information for these models includes a large margin of uncertainty. This spells a major task for the surveyor of results.

In the present investigation a comparison was made for only one non-equilibrium situation. For this purpose the theoretical results of Hall *et al.* (1962) were selected, partly because of their freedom from restrictive assumptions, and also because they have served as a standard for other authors. Of present interest are the results corresponding to an altitude of 150 kiloft., free-stream speed of 15,000 ft./sec, and nose radius of 0·183 ft. Hall *et al.* used full air chemistry for flow behind a catenary shock. This differs from the present simplified chemistry, but for the given free-stream conditions most of the chemical effects come from the dissociation of oxygen, which is presently accounted for. For this case Hall's rate and equilibrium constants were used. As for the catenary shock, upon inspection it proves to be very close to a circle for angles well past $\theta = 9{\cdot}2$ degrees, where the comparison is made. Results are shown in figure 14. The largest discrepancy is in the degree of dissociation (fraction of atomic oxygen) and is due to Hall's inclusion of NO reactions, which are disregarded in the present work. A rough way of accounting for the oxygen involved in NO is simply to add it to the atomic oxygen, in which case the top curve is obtained. Temperature and density are in very good agreement with Hall's results. The discrepancy near the body is undoubtedly due to the more complex oxygen exchange in Hall's reactions.

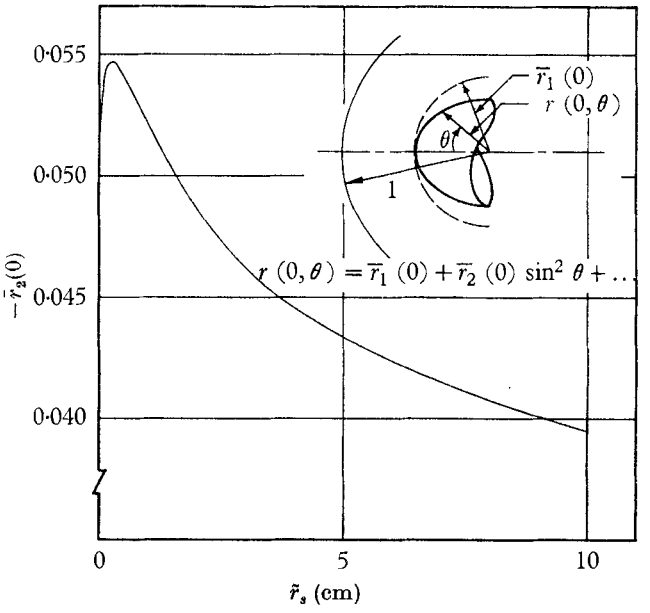

FIGURE 13. Body shape.

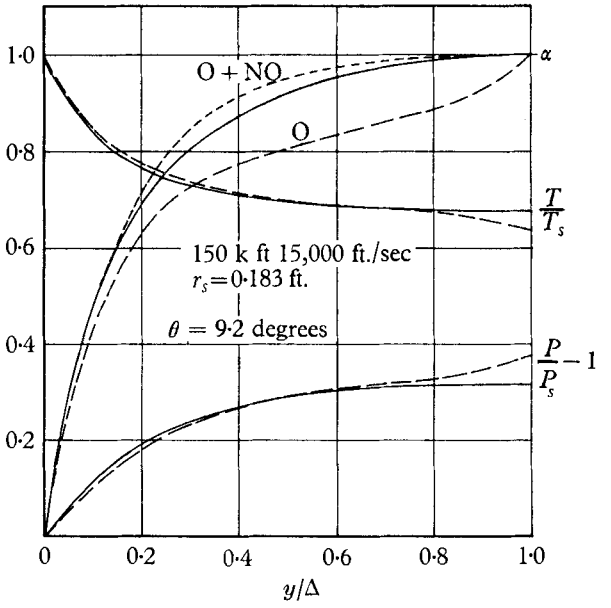

FIGURE 14. Comparison of results. Hall's results are shown in broken lines, the present results in solid lines. The co-ordinate y is a radial distance measured from the shock.

4. Conclusions

The method of series truncation provides a relatively simple way of analysing non-equilibrium blunt-body flows without the benefit of hypersonic simplifications. One works with ordinary differential equations, which is a marked advantage since numerical integration is then a matter of simple routine. As

an added benefit a powerful resolution of the flow field is obtained because of the arbitrarily small integration mesh. This allows the user to cope with the drastic changes in chemical and thermodynamic variables existing across the blunt-body non-equilibrium flow field.

First-approximation results are easy to obtain, and systematic improvement is an inherent feature of the scheme. A careful choice of variables and expansions minimizes the truncation error stemming from the elliptic nature of the subsonic flow equations. In this sense, pressure is to be preferred over density as a working variable. The electronic computer is used sparingly, and results bear semi-analytic representation. A shortcoming exists in the need for analyticity—or at least 'smoothness'—of the flow field in order to represent it far from the axis.

In the present investigation this method was used to analyse a wide range of non-equilibrium régimes. In particular, near-frozen flows were followed to the vicinity of the stagnation point through large gradients of temperature and composition. In this region reacting flows are better analysed in terms of temperature. The present computations show good evidence that equilibrium is actually attained at the stagnation point.

As non-equilibrium régimes in the shock layer approach the frozen limit, the final state of equilibrium changes almost imperceptibly. However, in the frozen limit there is a sudden jump to perfect-gas values at the wall. This singular nature of the frozen limit underlies the equilibrium drive taking place at constant pressure near the wall. The situation is reminiscent of Prandtl's boundary layer, which is associated with the singular limit of zero viscosity. The development along the body of an entropy layer due to the equilibrium-drive phenomenon is a question open to further research.

The present work was supported by the U.S. Air Force Office of Scientific Research under Contract No. AF 49(638)-1280. The author is indebted to M. D. Van Dyke for his advice and criticisms. Discussions with W. G. Vincenti and H. K. Cheng were also of great help.

REFERENCES

BELOTSERKOVSKII, O. M. & DUSHIN, V. K. 1964 Nonequilibrium supersonic gas flow around blunt bodies. *Zh. Vych. Mat. i Matem. Fiz.* **4**, 61.

BLOOM, M. H. & STEIGER, M. H. 1960 Inviscid flow with non-equilibrium molecular dissociation for pressure distributions encountered in hypersonic flight. *J. Aerospace Sci.* **27**, 821.

BLYTHE, P. A. 1963 The effects of vibrational relaxation on hypersonic flow past blunt bodies. *Aer. Quart.* **14**, 357.

CHUNG, PAUL 1961 Hypersonic viscous shock layer of nonequilibrium dissociating gas. *NASA TR* no. R-109.

CONTI, R. J. 1964 Stagnation equilibrium layer in nonequilibrium blunt-body flows. *AIAA J.* **2**, 2044.

ELLINGTON, D. 1963 An approximate method for calculating hypersonic nonequilibrium airflows past blunt bodies. *Canad. Arm. Res. and Dev. Establ. TR* no. 458/63.

FREEMAN, N. C. 1958 Non-equilibrium flow of an ideal dissociating gas. *J. Fluid Mech.* **4**, 407.

GIBSON, W. E. & MARRONE, P. V. 1962 A similitude for nonequilibrium phenomena in hypersonic flight. AGARD Meeting on high Temperature Aspects of Hyp. Fluid Dyn., Brussels, Belgium, April 1962.

HALL, J. G., ESCHENROEDER, A. Q. & MARRONE, P. V. 1962 Blunt-nose inviscid airflows with coupled nonequilibrium processes. *J. Aero Sci.* **29**, 1038.

HAYES, D. H. & PROBSTEIN, R. F. 1959 *Hypersonic Flow Theory.* New York: Academic Press.

KAO, H. C. 1964 Hypersonic viscous flow near the stagnation streamline of a blunt body. *AIAA J.* **2**, 1892.

LEE, R. H. & CHU, S. T. 1964 Nonequilibrium inviscid flow about blunt bodies. *Aerospace Corp.* SSD-TDR-63-369.

LICK, W. 1960 Inviscid flow of a reacting mixture of gases around a blunt body. *J. Fluid Mech.* **7**, 128.

LIN, S. C. & TEARE, J. D. 1961 A streamtube approximation for calculation of reaction rates in the inviscid flow field of hypersonic objects. *6th Symp. on Ballistic Mis. and Aer. Tech.*, vol. 4. New York: Academic Press.

LUN'KIN, IU. P. & POPOV, F. D. 1964 Influence of nonequilibrium dissociation on supersonic flow around blunt bodies. *Zh. Vych. Mat. i Matem. Fiz.* **4**, 896.

MARRONE, P. V. 1963 Inviscid, nonequilibrium flow behind bow and normal shock waves, Part I. *Cornell Aer. Lab. Rep.* no. QM-1626-A-12(I).

MURZINOV, I. N. 1961 The flow of gas near the stagnation point of a blunt body with a finite rate of excitation of vibrational degrees of freedom. *Akad. Nauk SSSR Mek. i Mashin.*, no. 6, p. 33.

SCHLICHTING, H. 1960 *Boundary Layer Theory*, p. 146 (4th ed.). New York: McGraw-Hill.

SHIH, W. C. L. & BARON, J. R. 1964 Nonequilibrium blunt-body flow using the method of integral relations. *AIAA J.* **2**, 1062.

SPRINGFIELD, J. F. 1964 Steady, inviscid flow of a relaxing gas about a blunt body with supersonic velocity. *1964 Heat Tr. and Fl. Mech. Inst.*, p. 182. Stanford University Press.

SWIGART, R. J. 1962 A theory of asymmetric hypersonic blunt-body flows. *Stanford U. SUDAER* no. 120; also *AIAA J.* **1**, 1034.

VAN DYKE, M. D. 1964*a* The blunt-body problem revisited. *Internat. Hyp. Symp., Buffalo, N.Y.*, 25 June 1964.

VAN DYKE, M. D. 1964*b* The circle at low Reynolds number as a test of the method of series truncation. *11th Internat. Congress of Appl. Mech., Munich*, 30 August 1964.